Wei Gao
School of Mechanical Engineering,
Purdue University,
West Lafayette, IN 47907
e-mail: gao51@purdue.edu

Karthik Ramani
School of Mechanical Engineering,
School of Electrical and Computer
Engineering (by courtesy),
Purdue University,
West Lafayette, IN 47907
e-mail: ramani@purdue.edu

Raymond J. Cipra
e-mail: cipra@purdue.edu

Thomas Siegmund
e-mail: siegmund@ecn.purdue.edu

School of Mechanical Engineering,
Purdue University,
West Lafayette, IN 47907

Kinetogami: A Reconfigurable, Combinatorial, and Printable Sheet Folding

As an ancient paper craft originating from Japan, origami has been naturally embedded and contextualized in a variety of applications in the fields of mathematics, engineering, food packaging, and biological design. The computational and manufacturing capabilities today urge us to develop significantly new forms of folding as well as different materials for folding. In this paper, by allowing line cuts with crease patterns and creating folded hinges across basic structural units (BSU), typically not done in origami, we achieve a new multiprimitive folding framework such as using tetrahedral, cuboidal, prismatic, and pyramidal components, called "Kinetogami." "Kinetogami" enables one to fold up closed-loop(s) polyhedral mechanisms (linkages) with multi-degree-of-freedom and self-deployable characteristics in a single build. This paper discusses a set of mathematical and design theories to enable design of 3D structures and mechanisms all folded from preplanned printed sheet materials. We present prototypical exploration of folding polyhedral mechanisms in a hierarchical manner as well as their transformations through reconfiguration that reorients the material and structure. The explicit 2D fabrication layout and construction rules are visually parameterized for geometric properties to ensure a continuous folding motion free of intersection. As a demonstration artifact, a multimaterial sheet is 3D printed with elastomeric flexure hinges connecting the rigid plastic facets. [DOI: 10.1115/1.4025506]

1 Introduction

Origami originally was developed as a paper craft in the 17th century AD that allowed the diversity of representative 3D objects with individual unit arrangements and explicit folding processes from 2D sheets of paper. Artistic origami designs reveal the rudimentary characteristics of paper folding: inexpensive, lightweight, compact, and combinatorial. During the last 40 yr, "Why's, What's, and How's" of different origami tessellations and structures have been geometrically and symbolically described by the underlying mathematical rules governing the creases, such as flat foldability [1] and "folding any polygonal shape" [2]. With the marriage of computational geometry and origami, systematic studies have been carried out recently (TreeMaker [3], Origamizer [4]).

Our analysis of past work in origami and folding structures shows that its applications are limited by the following characteristics: (1) A number of developments have the typical goal of achieving a desired folding-state that renders functionality, i.e., the extended solar panel or the wrapped gift package. (2) In the previous work, continuous skin-based models and patterns are achieved by task-oriented operations (Miura folding [5] as well as patterns represented in airbag [6], stent [7], sandwich core structures [8], and cartons [9]). (3) Recent advances in modular origami [10] as well as its variation modular kirigami [11] for polyhedral models use separate pieces of paper for each component or function. The designers still face the uncertainties of building combinatorial systems out of single folded sheets, and of placing material where they desire it.

Recent literature has shown and proved that a linear chain of polygonal or polyhedral modules can be folded into any arbitrary 3D shape [12,13] and reach many general families of hinged dissection [14,15]. Our vision herein is to enable a new multiprimitive folding framework with analogous 3D folding schemes and 2D fabrication routines, to specifically fold closed-loop(s) polyhedral mechanisms (linkages) with multi-degree-of-freedom and self-deployable characteristics, we call "Kinetogami." We coined the word "Kinetogami" inspired by the Greek root "Kinetikos" and the Japanese word "kami", literally meaning that the polyhedral mechanisms and structures in motion are made by a single sheet of paper.

Polyhedral mechanisms are spatial mechanisms where vertices, edges and facets of the polyhedra are embedded into fundamental kinematic linkages and closed chains [16]. In physical kinematic linkage design, each link is modeled as a rigid body and these individual links are jointed together in closed form(s) to provide a particular determinate motion. We specifically investigate sets of periodic polyhedral pairs with reflectional symmetry and adjacent hinge axes with skew perpendicularity in the kinematic chain(s). In an analogous manner, we fold and close polyhedral facets to construct *"Basic Structural Units"* in a way that each individual polyhedron can be represented as a rigid link while maintaining the hinge axes orientations. These folded "links" are structural with empty volume enclosed instead of solid rods. The resulting mechanisms can reconfigure and manifest different functions afforded by the new configuration. Our design methodology allows manufacturing in 2D and folding in 3D.

Our design construction theories and specific procedures for our systematic folding framework are sequenced as follows:

(1) forming a class of elementary BSUs using tetrahedral, cubic, prismatic, and pyramidal components (Sec. 2);
(2) synthesizing the 2D crease-cut-attachment patterns for each BSU and modifying the design parameters to allow reconfigurability (Secs. 2 and 4);
(3) linearly extending a single BSU unfolded pattern along the long strip of sheet and sequentially folding each pattern up into a string (Sec. 5);
(4) threading the string through an Eulerian cycle where the generalized algorithm is verified (Sec. 5), and
(5) attaching all the compound joints together while closing each individual loop (Sec. 5).

Contributed by the Design Automation Committee of ASME for publication in the Journal of Mechanical Design. Manuscript received February 1, 2013; final manuscript received September 4, 2013; published online October 8, 2013. Assoc. Editor: Alexander Slocum.

Hence, by synthesizing and modifying the geometric features embedded in the 2D crease-cut-attachment patterns, we hierarchically change the kinematic performance of the single/multiclosed-loop reconfigurable polyhedral mechanisms to be folded, and finally, provide the capacities for rendering different functionalities by changing locking/unlocking, loading/unloading, and locomotive behaviors from a mechanical engineering design point of view. The use of paper-like, multimaterial substrates via 3D printing further achieves efficient fabrication and packaging (Sec. 6). To the best of our knowledge, such hierarchical and multiscale mechanism constructions through folding and reconfiguration have not been envisioned or explored earlier.

2 Formation of Basic Structural Units

In the past, the nature of paper sheets was deterministic with regard to the conventional rules of origami such as when folding without cutting. We strive toward exploring the heterogeneous, structural, and reconfigurable characteristics of paper by allowing preplanned cuts with crease patterns and creating folded hinges across basic structural units, typically not done in Origami.

In our work, nondeformable paper sheets are used to construct the basic structural units. We model the creases as revolute joints (hinges), the increased facets as polyhedral surfaces and closed-form surfaces as component links. Line-cuts are necessitated for silhouetting the unfolded pattern of each polyhedral linkage and the attachments on each unfolded BSU pattern are considered as the post processing to close physical volumetric unit as a rigid body. Generally speaking, a BSU consists of a pair of mirror-image polyhedra coupled with a common hinge. Furthermore, the BSUs can be folded and strung up from extending crease patterns laterally on a single flat sheet of paper. Here, we demonstrate four representative BSU's: tetrahedral, cuboidal, prismatic, and pyramidal (shown in Fig. 1) stemming from the folding-cutting-joining processes on 2D sheets.

Our BSU folding approach provides advantages such that: (1) The hinges are inherently embedded as the creases on the 2D pattern. Hence, no assemblages of separate joints are needed to construct the mechanism. (2) The internal space inside each BSU can be utilized for added functions, such as enclosing electronic and battery components for actuation. (3) Affording opportunities for planning anisotropic material properties on a unfolding pattern while the reconfigurability in mechanisms reorients the material and structure and thereby changes functionalities.

2.1 Tetrahedral BSUs. Four triangular facets and six edges comprise a tetrahedral unit. In order to form a closed tetrahedron, each set of unfolded triangle patches needs to maintain (a) the edge-length consistency: any side length of each triangle must agree with the one to be joined from the other three triangles, respectively (i.e., in Fig. 2(*a*): $a = a', b = b', c = c'$), and (b) the vertex-angle consistency: the sum of angles spanned by adjacent edges emanating from the vertex must be less than 2π, i.e., $\alpha + \beta + \gamma < 2\pi$. This arises from the fact that if the sum is equal to 2π, a tetrahedron converts to a plane; and if greater than 2π, a tetrahedron is not formable.

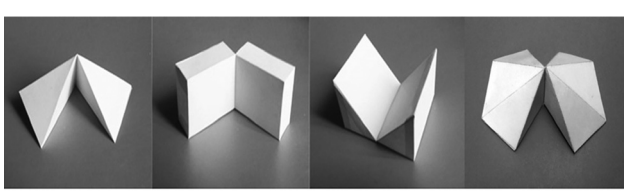

Fig. 1 Four representative ((*a*): tetrahedral; (*b*): cuboidal; (*c*): prismatic; (*d*): pyramidal) BSUs folded from a single sheet.

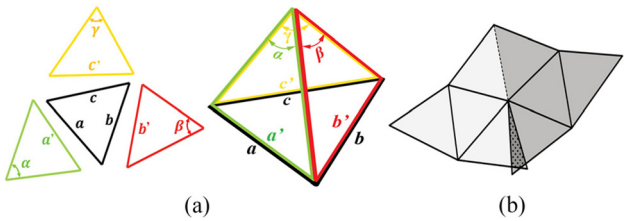

Fig. 2 (*a*) 2D-3D formation of a single tetrahedral unit. (*b*) Self-overlapping on a unfolded tetrahedral BSU pattern.

Coupled mirror-image tetrahedra with a common hinge are labeled as a tetrahedral BSU. In general, while flattening each BSU, single paper consumption requires none of any two neighboring facets overlaps upon each other (dotted areas in Fig. 2(*b*)). By unfolding a single polyhedral unit, we allow only 2 hinge edges on the pattern such that one hinge connects to the previous unit and the other connects to the next unit. Therefore, we predesign the hinge edges in a parallel manner and the unfolding net of each current unit is in between the adjacent hinges. Given that BSUs with reflectional symmetry are periodically chained together, we are guaranteed to avoid self-overlapping pairs of adjacent facets after opening polyhedral BSUs into a 2D plane.

Figure 3 shows 3 representative tetrahedral BSUs where each sides' geometry are: all isosceles triangles (shown as a: isosceles tetrahedron); all right-angle triangles of which edges are in the ratio of $1 : \sqrt{3} : 2 : \sqrt{5} : 2 : 1$ (b: skew tetrahedron); and the one having isosceles, equilateral and right-angle triangles with edge ratios of $1 : 2 : \sqrt{5} : 2 : \sqrt{5} : 2$ (c: isos-equal tetrahedron). Their corresponding 2D crease patterns are shown in Fig. 3.

A closed loop of serially connected BSUs (necessarily identical to each other) is defined as a *BSU ring*. In this kinematic chain, any two neighboring polyhedra can be viewed as a BSU. Geometrically speaking, in a tetrahedral BSU ring, 2 adjacent hinge axes are skew perpendicular, and 2 alternate ones intersect at a common point. More complex tetrahedral mechanisms with multiple degrees of freedom can be achieved using serial, parallel, and hybrid assemblies of BSU rings in a hierarchical manner.

2.2 Cuboidal BSUs. A number of engineering design practices [17,18] have been recently revisiting the simple, combinatorial, and space-efficient structure: the cuboid. Each cuboidal unit (including the cubic one) contains 12 edges and 6 surfaces while its flattened pattern opens up to 14 edges along the path

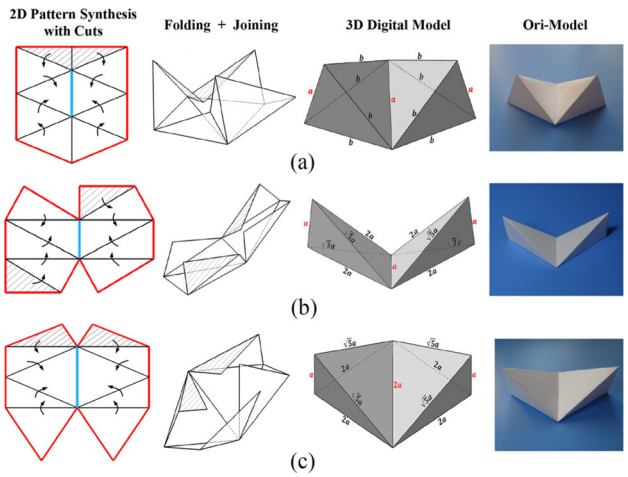

Fig. 3 (*a*) Isosceles tetrahedral BSU; (*b*) skew tetrahedral BSU; (*c*) isos-equal tetrahedral BSU (*red*: overall cuts; *black*: folds; *blue*: the fold that functions as a common hinge; *shaded area*: attachments)

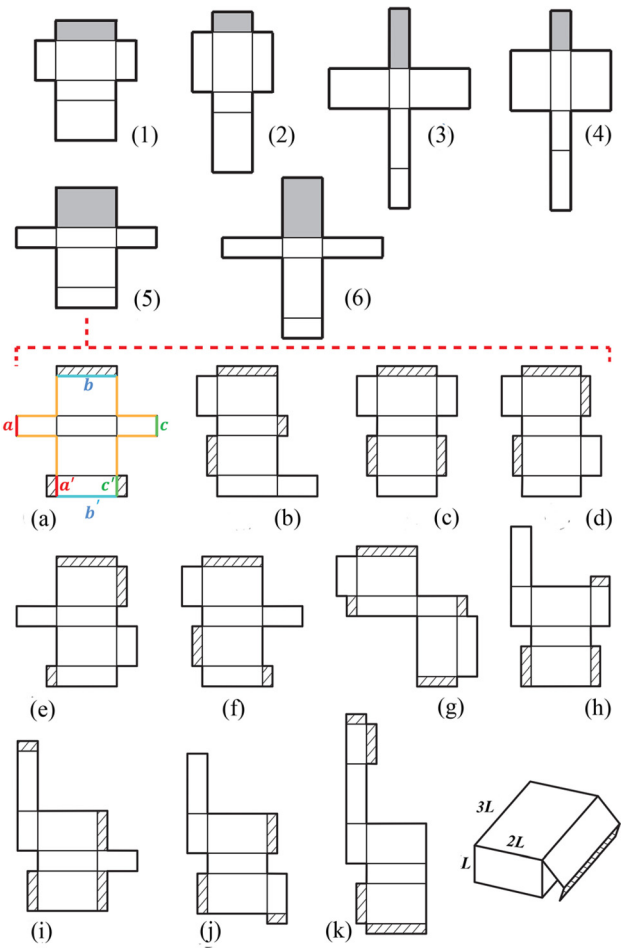

Fig. 4 54 unique 2D crease patterns with attaching facets for a cuboidal unit (6 parent patterns with a corresponding child pattern are shown)

surrounding the area. In accordance with 11 different planar nets of a cube [1], we start with various 2D patterns for constructing a single cuboidal unit (cuboidal edges are in the ratio of 3 : 2 : 1) and embed them with the attaching facets for gluing. When considering a cross-like shape as a parent pattern, we obtain six different layouts by arranging orientations of the top middle rectangles in grey (we call the base, shown in Fig. 4 (1–6)). Each layout yields 11 unique child patterns (see Figs. 4(*a*)–4(*k*) for the parent 5) referring to the same base's orientation. Note that the parent patterns are the patterns with the same net while altering the shape of each base rectangle. The child patterns are the ones with the same base rectangle while altering the nets. We eventually generate a total of 66 2D crease patterns in general to fold a cuboid with 12 patterns forming identical pairs.

The displacement and orientation arrangement of each attaching facet are based on the premise that we minimize the overall paper consumption (envelope size of each pattern) as well as the number of attaching facets. For instance the pattern (a) in Fig. 4, the two same colored edges (nonadjacent sets in red (a, a'), blue (b, b'), green (c, c'), and adjacent ones in yellow) coincide with each other after folding the net up to a closed cuboid. We arrange and extend 3 attaching facets out of nonadjacent sets so that the cuboid can be enclosed efficiently without any curled-up corner.

Similar to the tetrahedral BSU formation, the net pattern for a cuboidal BSU can be eased out of a single piece of paper when (1) the hinge to be chosen out of three nonadjacent sets on one cuboidal unit pattern matches the one on the coupled pattern; (2) no self-overlapping occurs after combining two individual nets together; and (3) two built-up cuboidal units are symmetric about

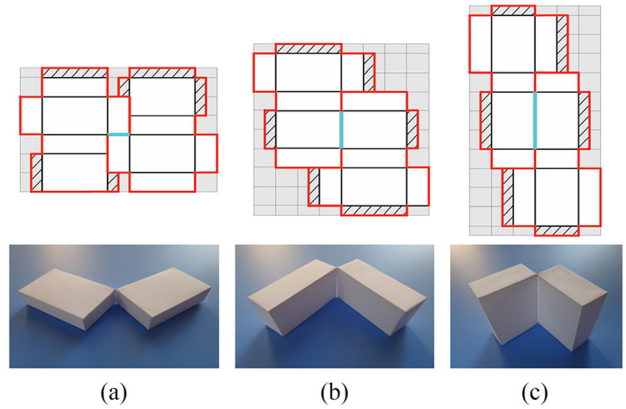

Fig. 5 Net patterns of cuboidal BSU using three different edges as hinges (*red*: overall cuts; *black*: folds; *blue*: the common hinge)

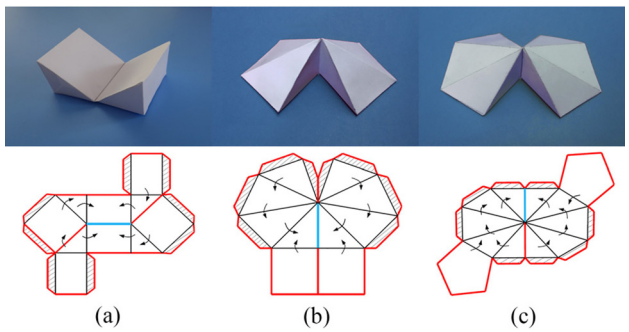

Fig. 6 (*a*) Triangular prismatic BSU; (*b*) rectangular pyramidal BSU; and (*c*) pentagonal pyramidal BSU

the common hinge axis. We synthesize 3 net patterns by picking an edge along the length, width, and height individually as the common hinge. We use the most compact envelop area by brute-force searching to chose candidates from a total of 54^2 combinatorial possibilities for attaching-facet arrangement. Figure 5 also shows the hands-on prototype corresponding to each cuboidal net pattern. Note again that a cuboidal BSU ring is a closed-loop chain with coupled cuboidal BSUs and in which the adjacent hinge axes are skew perpendicular to each other.

2.3 Prismatic and Pyramidal BSUs. Another two representative modules in the family encompass prismatic and pyramidal BSUs. Consider the (a) triangular prismatic, (b) rectangular, and (c) pentagonal pyramidal BSUs in Fig. 6, each BSU consists of two mirror-image units with n-sided polygonal bases. In each unit, either a side edge or a base edge with skew perpendicularity can be selected as the common hinge edge. Observe that in these unfolded nets, the attaching areas are extended from a single side of each prism face and faces surrounding the apex in pyramidal BSUs.

3 Hierarchies and Combinatorics of Depolyable Kinetogamic Derivatives

Schatz [19] in 1929 first invented the single closed chain with an even number of symmetric tetrahedra. Schattschneider and Walker later decorated the tetrahedra chains and called it Kaleidocycle [20]. A ring hinged with 3 tetrahedral BSUs can be simplified into 6 rigid rods, the deployable mechanism is named threefold symmetric Bricard linkage with 1 DOF [21]. The parallel mechanism with multiple loops, however, becomes a challenge for engineers to synthesize and even to perceive.

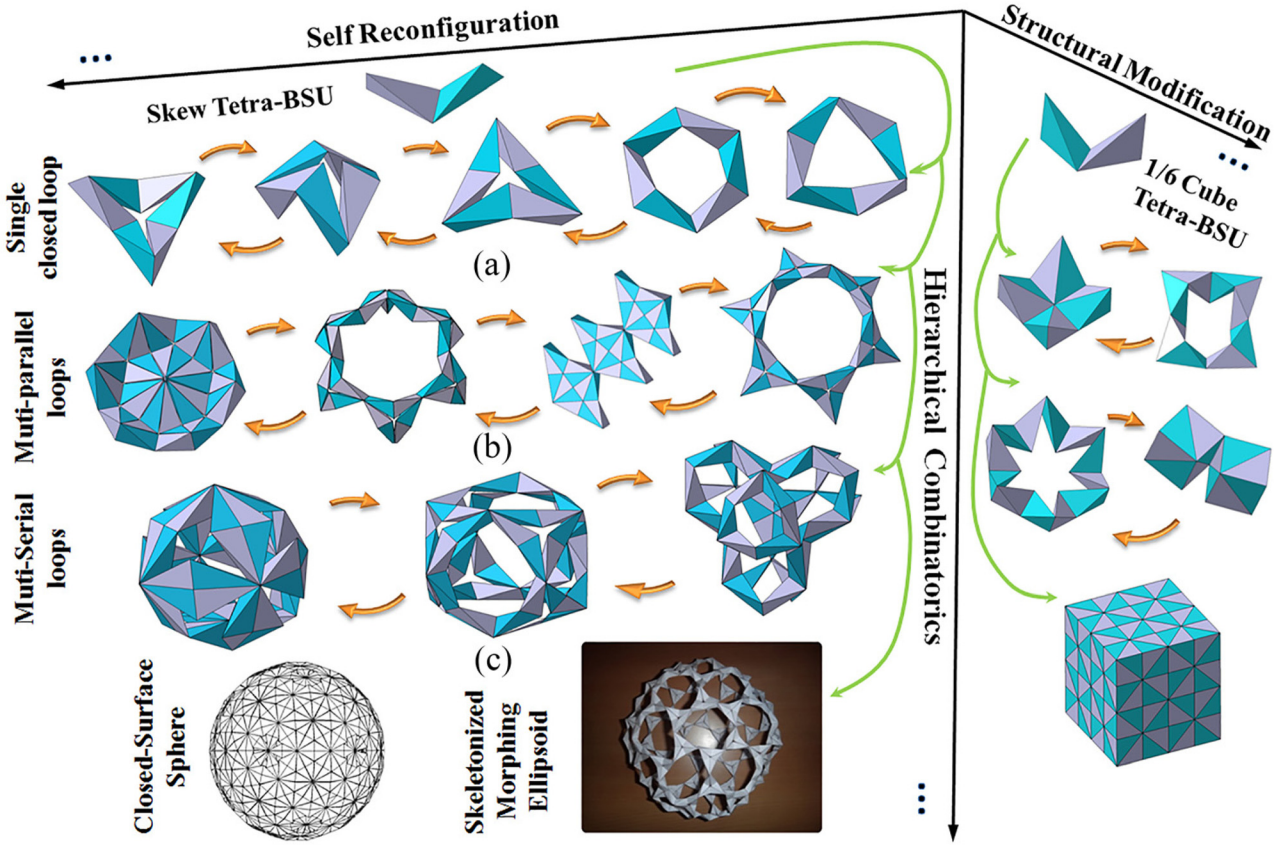

Fig. 7 Kinematical combinatorics of tetrahedral BSUs

In the formation Sec. 2, the representatives for each primitive BSU were geometrically chosen based on a main feature that the two adjacent hinge axes in each unit are skew perpendicular to each other. Next, we sequentially connect mirror-image BSUs into closed loop(s) so that each loop fulfils the plane-symmetric and trihedral linkage conditions [22,23], and accordingly, results in a deployable kinematic property. We demonstrate herein the hierarchical architecture of reconfigurable polyhedral mechanisms derived from BSUs. Starting from a single BSU, higher level locomotion is enabled by using serial, parallel, and hybrid assemblies. Each derived structure and mechanism can be considered as a new BSU to repetitively or cumulatively achieve more complicated ones, while at each generation the construct is capable of self-reconfiguring among multiple configurations and folding states.

For an explicit demonstration, skew tetrahedral BSU (we call stBSU, see Fig. 3(*b*)) as a basis turns out to be combinatorial and topological in both structural and kinematic perspectives. The shown white and blue units are mutually symmetric in a BSU. By connecting three skew tetrahedral BSUs in a serial closed loop (we call 3stBSU), we form a equilateral-triangle-like structure (see "Single closed loop" in Fig. 7). Hinging six 3stBSUs serially further gives a closed-surface hexagon-like structure shown in "Multi-Serial-Loops" of Fig. 7 and the paper model in Fig. 8(*b*). The 3stBSU can be reconfigured to a zigzag mechanism and the hexagram-like mechanism with unfilled central space (see "Multi-Serial-Loops" in Fig. 6 and the paper model in Fig. 8(*f*)). By initializing one configuration of each reconfigurable BSU and building them up cumulatively, it gives rise to versatile rigid structures and movable mechanisms, i.e., the closed-surface sphere in Fig. 7 with overall 540 tetrahedral BSUs with paper model shown in Fig. 8(*c*), and the skeletonized morphing ellipsoid with overall 216 stBSUs (see the paper model in Fig. 8(*h*)). Given a total of 180 stBSUs, we also achieved a closed-surface ellipsoid in Fig. 8(*d*) with varying compliance in different sections. Eventually, modifying the size of BSUs enables different solid structures with overall 192 tetrahedral BSUs to be transformed as well (see the derivatives in "Structural Modification" section of Fig. 7). Gao et al. [24] presented a hexapod locomotive robot by stringing up 3 skew tetrahedral BSUs as each limb and connecting 6 3stBSUs serially. Three potential gaits patterns are also simulated for the robot: squatting/rising, squirming, and slithering.

The analogical closed-loop(s) mechanism construction and self-deployable kinematic characteristics are also investigated using cubic BSUs. Many algorithmic and programmable approaches have considered how to fold a linear chain of cubes and achieve any polycube shape [12,13]. The work demonstrated here is different because our approach lays out hinge orientation on 2D, folds cubic BSU strings into closed loop(s) to construct kinematic mechanisms. Starting from a single cubic BSU, one can join n identical BSUs in a closed loop while alternating successive hinge orientations with a degree of perpendicularity. By satisfying the plane-symmetric and trihedral linkage conditions [23], it gives construction of serial cubic mechanisms that reveal the same self-deployable properties (case $n=3$ are show in Figs. (8(*i*) and 8(*j*)) and case $n=4$ are show in Figs. (8(*k*) and 8(*l*)). In Fig. 8(*m*), the mechanism consisting of 3 cuboidal BSUs (cuboidal edges are in the ratio of $3:2:1$) is able to deploy (see Fig. 8(*n*)) into the triangle-like configuration in Fig. 8(*o*). The same self-deployable performance is exploited using the prismatic and pyramidal BSU rings shown in Figs. 8(*p*)–8(*s*)). Therefore, we show the proof of concept of our prototypical experiments and we will detail the kinematic analysis of each polyhedral mechanism in our subsequent work.

4 The Synthesis of Reconfigurability

The advantages of reconfiguration in "Kinetogami" are twofold and highly coupled. It is based on both the ease of fabricating in

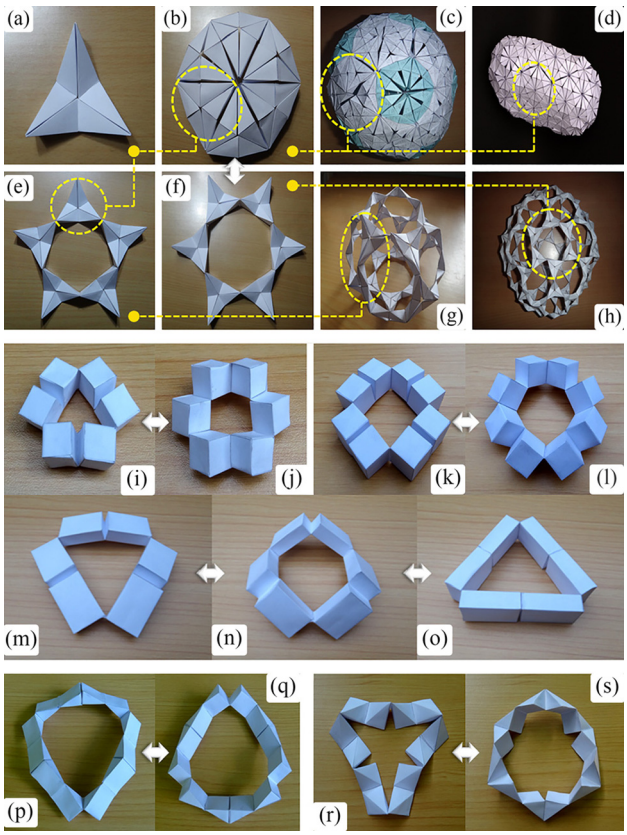

Fig. 8 Prototypical Kinetogamic derivatives from 4 BSUs: (*a*)–(*h*) constructs using tetrahedral BSUs. (*i*)–(*o*) constructs using cubic/cuboidal BSUs, (*p*) and (*q*) constructs using prismatic BSUs, (*r*) and (*s*) constructs using pyramidal BSUs

2D followed by folding to 3D, and the highly efficient reconfiguration between mechanisms and structures, which provides affordances for changing behaviors, such as load carrying capacities or locomotion capacities. Locking the global or the local zones provides both mobility and rigidity of 3D mechanisms in scalable engineering systems. Folding mechanisms are used initially with cutting and gluing to form the baseline topology of the device, and unfolding and ungluing can be used during operation of the device to change the baseline topology. We now develop the methodology to map mechanism's reconfigurability into 2D crease-cuts-attachment layout designs and pipeline systematic procedures to complete our folding framework.

It is a difficult task to describe and predict the possible variation of configuration states (Ω) during the folding operation on flat sheets. Continuous, restricted, and prohibitive rotations were observed within Kaleidocycle structures. We therefore propose a predictor of reconfigurability by concentrating on spatial perception and engineering-domain knowledge. The reconfigurability here is defined as the ability of a BSU ring to perform the "full body" rotation. Thus, one can design a desired motion of morphing structures and reconfigurable mechanisms using measurable design parameters.

The synthesis rules are processes developed by evaluating the vertex angle of each side of an isosceles tetrahedral BSU. For a tetrahedral BSU ring, each tetrahedral unit is interpreted as a common normal of its two skew perpendicular joint axes, called a "rotating rod" represented as the dashed red line segment *EF* in Fig. 9).

This predictor of reconfigurability, θ, is an intrinsic and measurable characteristic parameterized in the flat pattern with four identical isosceles triangles, as shown in Fig. 3(*a*). It can be defined if a single closed BSU ring is able to rotate continuously, with a limited range or become a rigid structural body by the following reasoning: Let the half base length ($AB/2$ or $CD/2$) be

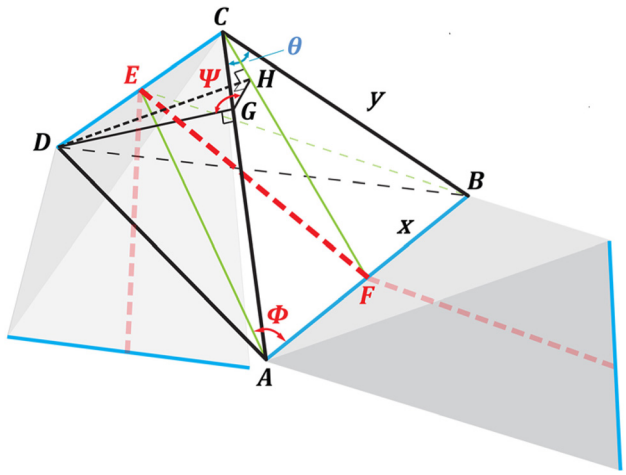

Fig. 9 Geometric parameters for determining variation of configuration states

x, and equal side length (AC, AD, BC, BD) be y, therefore $\theta = 2\arcsin(x/y)$. Identification of θ arises by solving equations in two particular cases shown below, while increasing the vertex angle θ from zero

- if the angle $\Phi = \angle(AB, ACD)$ remains larger than the threshold value $360\,\text{deg}/2n$ (see Eq. (1)), where n is the number of isosceles tetrahedral BSUs in the ring, then the single ring is capable of performing a full body rotation. This arises because the mechanism can pass through its singular configurations when all the tetrahedra gather toward the center. The threshold value for Φ is represented as

$$\Phi_{\text{Threshold}} = \arccos\frac{x}{\sqrt{y^2 - x^2}} = \frac{360}{2n} \tag{1}$$

- Afterward the ring performs a to-and-fro motion (no "full body" rotation) until the dihedral angle $\Psi = \angle(ABC, ACD)$ rises to $360\,\text{deg}/2n$. A rigid-body state is achieved right at the threshold value being satisfied (see Eq. (2)). It's because when the ring is folded, all internal tetrahedral surfaces meet and interfere with each other. The threshold value for Ψ can be represented as

$$\Psi_{\text{Threshold}} = \arcsin\frac{y\sqrt{y^2 - 2x^2}}{y^2 - x^2} = \frac{360}{2n} \tag{2}$$

These two equations lead to two threshold values for the predictor. For instance, the boundaries of the vertex angle in a chain of 3 isosceles tetrahedral BSUs are 53.13 deg and 70.53 deg for identifying and predicting a fully reconfigurable, limited reconfigurable or rigid body states (see Fig. 10(*a*)).

Extremal reachable values of θ allow us to define the range of 3 reconfigurable states, which are summarized as below in Eqs. (3)–(5) and lead to the corresponding plot in Fig. 11.

Rigid Body State

$$\theta = 2\arcsin\sqrt{\cot\frac{180}{n}\tan\frac{90}{n}} \tag{3}$$

Limited Reconfigurable State

$$2\arcsin\frac{1}{\sqrt{\tan^2\frac{180}{n} + 2}} < \theta < 2\arcsin\sqrt{\cot\frac{180}{n}\tan\frac{90}{n}} \tag{4}$$

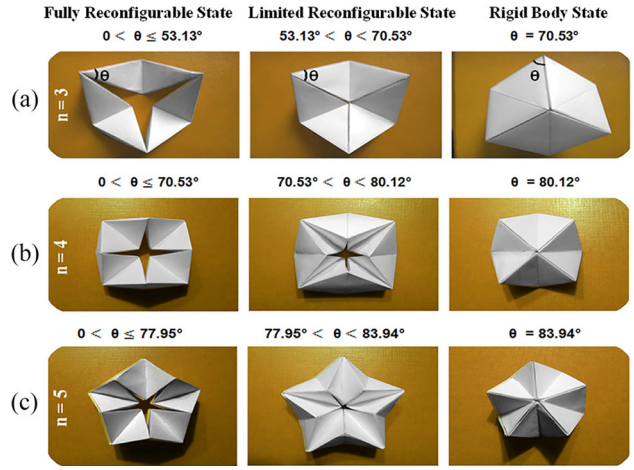

Fig. 10 Prototypical demonstration of fully, limited reconfigurable, and rigid-body state: single ring (*a*) with 3 isosceles tetra-BSUs, (*b*) with 4 isosceles tetra-BSUs, and (*c*) with 5 isosceles tetra-BSUs

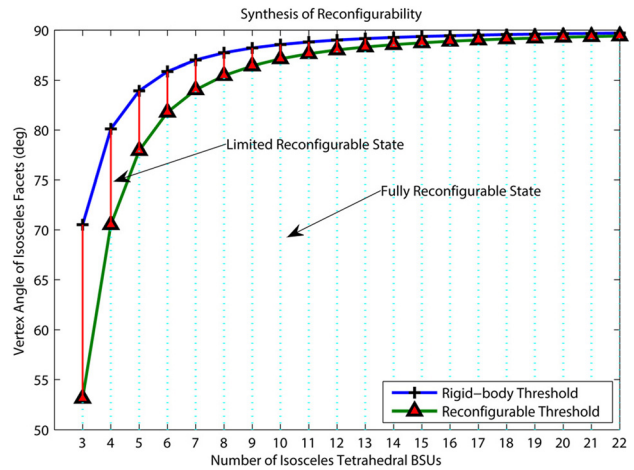

Fig. 11 Thresholds of fully, limited reconfigurable, and rigid-body state

Fully Reconfigurable State

$$0 < \theta \leq 2 \arcsin \frac{1}{\sqrt{\tan^2 \frac{180}{n} + 2}} \tag{5}$$

The plot shows a monotonically increasing region of the general reconfigurable state. Naturally, the final specification of the predictor θ depends on the choices of n. With the increase in the number of isosceles tetrahedral BSUs, one can expect a slow-growing space of fully-reconfigurable-states, and the rigid-body-state threshold for θ approaches (but never reaching) 90 deg. In general, the isosceles tetrahedral BSU string cannot be ringed if one continues to increase θ after reaching the rigid-body-state threshold. Note that the corresponding dihedral angle Ψ inside our presented cubic, prismatic and pyramidal units are fixed to be $\pi/2$, thus Eq.(2) indicates that a closed loop suffices to be formed given that the number of BSUs in the ring n is greater than 2.

5 2D Fabrication Principles and 3D Multimaterial Printing

5.1 Planning, Construction, and Folding. We develop consistent fabrication principles that can be applied to a flat sheet while exploring reconfigurable properties. Our folding approach is deployed on a single compact sheet to achieve Kinetogamic polyhedral mechanisms. We introduce the cuts into the crease pattern to provide skeletal structures therefore multiple folding states are enabled by configuring. Generalized reasoning and fabrication procedures are demonstrated in the case studies of constructing (1) a hexagram-like mechanism previously shown in Fig. 8(*f*) using stBSU, and (2) a deployable ring using cubic BSU.

5.1.1 Finding an Eulerian Cycle. In our multiprimitive folding scheme, all folded polyhedral mechanisms originate from a single linear BSU string. At this point, we first achieve the generalization of producing an Eulerian cycle that travels each BSU (linkages) exactly once for any kinetogami-derived polyhedral mechanism.

Cyclic hinged dissection has received multiple studies on finding a traceable path to form any polypolyhedra shape [14,15]. When considering the kinematic linkages, we start identifying the configuration space of the closed loop(s) polyhedral linkages. Milgram [25] discussed that closed loop revolute mechanisms have at least one planar configuration, a configuration that lies entirely in a single plane $R^2 \subset R^3$. Hence, the topological relationship of unfolded configuration of closed loop(s) polyhedral mechanisms can be described using a planar connectivity graph G. In the graph, polyhedral links are denoted by edges (–) and hinge joints (H) are denoted by *ordinary nodes* (○). Each ordinary node connects 2 links (edges) and it allows 1 rotational degree-of-freedom. When $k(k > 2)$ linkages are joined together while sharing a single hinge joint, this compound hinge joint (CH) is denoted by a *complex node* (◎) and it allows $k - 1$ revolute mobility. Each single basic-structural-units B_i is composed of two adjacent links Bi_{-1} and Bi_{-2} coupled together. If n basic-structural-units $B_1, B_2, \ldots, B_n$ are chained in a single closed loop shown in Fig. 12(*a*), it is defined as an *elementary-single-loop*. By picking arbitrary node(s) on each of m elementary-single-loops and joining them again to form compound hinges further give us a *multiloop in the order of m*. The multiloop construction guarantees nonintersecting edges given that each graph is a planar graph. Finally, we define that at any complex node, the two adjacent BSUs in the same elementary-single-loop are noted as a *pair* BSU*s*, such as B_i and B_j in Fig. 12(*b*), and the adjacent ones in the different elementary-single-loops are considered as a *dual* BSU*s*, such as B_i and B_k. Thus, at each complex node, on one side of any BSU must be its *pair* and the other side must be its *dual*.

The problem herein is described as follows: given a connectivity graph of multiloop in the order of m, where each elementary-single-loop consists of many basic structural units, to produce an Eulerian cycle which visits each BSU linkage exactly once. In order to tackle the problem, two operations are demonstrated as follows:

Operation1 *op1*(CH_i): Split each complex node (by the aforementioned multiloop definition, complex node is the compound hinge that couples k BSUs, k is even and $k \geq 4$) into $k/2$ divisions where the dual BSUs are connected together. The set of all newly-created ordinary nodes at each complex node position are defined

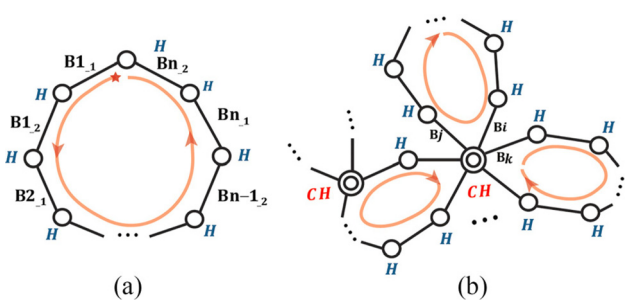

Fig. 12 (*a*) Elementary-single-loop with n basic-structural-units $B_1, B_2, \cdots, B_n$, (*b*) multiloop

as a *complex set*(CH_i). Hence, multiple cycles connecting nodes and edges will be generated.

Operation2 *op2*(CH_i): In an arbitrary *complex set*(CH_i), replace each BSU's connection to its dual back with a connection to its pair.

Algorithm 1. Find an Eulerian cycle that visits each BSU only once

Input: Given a connectivity graph G;

Step:

1: Find all the *complex nodes* in G

2: **for** each complex node (CH_i) **do**

op1(CH_i)

end for

3: **for** each *complex set* (CH_i) which is from different cycles **do**

op2(CH_i)

end for

Based on these two operations, our method to find an Eulerian cycle is summarized in Algorithm 1. The following is the detailed proof of the algorithm:

Proof. Recall that in each connectivity graph G, each ordinary node connects only two edges. Since the connectivity graph is a planar graph, we have the following two explicit results: (1) For Operation1, each newly created vertex where dual BSUs are jointed at in a *complex set* (CH_i) connects only two edges and it becomes an ordinary node. The process retains the planar properties. (2) For Operation 2, each newly created vertex after pair BSUs are coupled back also connects only two edges. These vertices become an ordinary node and it also retains the planar properties.

After Step 2 completes (for each *complex node* (CH_i), we do the Operation 1), given that each node in the obtained graph G connects two edges, the obtained graph G only comprises of one or multiple cycles connecting nodes and edges. In each cycle, every node connects only two edges. Because the connectivity graph is a planar graph and the Operation1 retains the planar properties, these cycles do not intersect with each other. Then, we proceed to Step 3.

Note that each newly created node after Operation 2 still connects two edges. Therefore, after step 3, all the ordinary nodes in the obtained final graph G' still have only two edges connected on each side. That is, G' is composed of one or multiple cycles. However, since the original connectivity graph contains only one connected component, step3 ensures that it results in only one single non-intersecting cycle. This is due to the fact that if there exist multiple cycles, then we can return back to Operation 2 to merge them. Thus, the resulting final graph G' by this algorithm is a single Eulerian cycle without self-intersection. Figure 13 shows the hexagram-like mechanism previously illustrated in Fig. 8(*f*), which has a total of six complex nodes *CHs*, where four BSUs, such as B_1, B_3, B_4, and B_5, are hinged together at each *CH*. Step 2 isolates 2 dual BSU pairs (B_1, B_4 as a dual and B_3, B_5 as another) and generates 2 new cycles where each ordinary node connects only two edges. Finally, replacing each BSU's connection back to its pair (B_1 hinges to B_3, and B_4 hinges to B_5) results in an Eulerian cycle for the mechanism.

As for the time complexity of this algorithm, it is $O(m+n)$, where m is the number of the nodes and n is the number of edges in G. Therefore, once again, any resulting connectivity graph can become a single closed cycle and the Eulerian path is found with a long nonintersecting BSU string.

5.1.2 Fundamental Reasoning. For both of these case studies, the construction rules are generalized through the following sequences:

(1) Duplicate the single crease pattern of skew tetrahedral BSU (see the grey area in Fig. 14(*a*)) and cubic BSU given in Fig. 15(*b*) so that one can linearly extend them along a strip

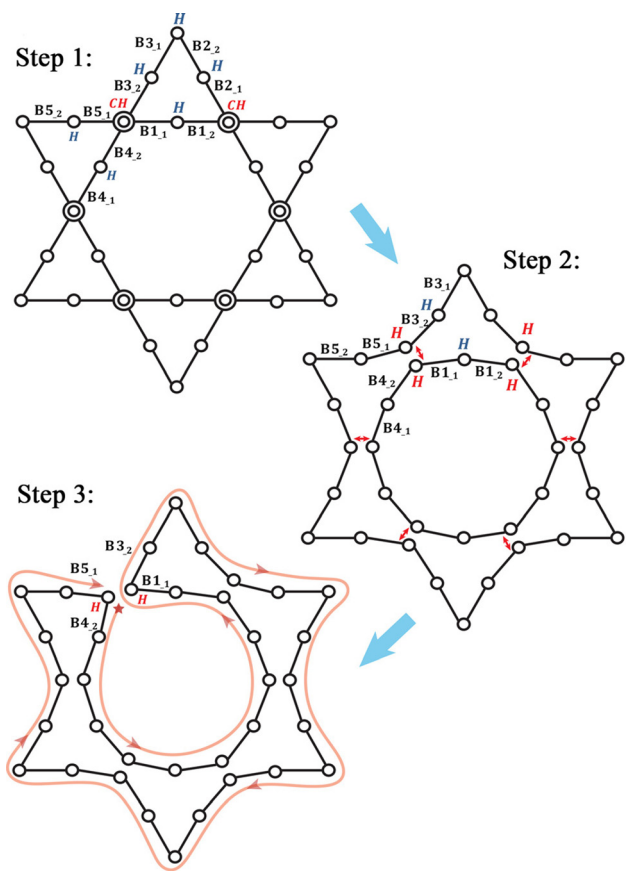

Fig. 13 Eulerian cycle generation for a hexagram-like mechanism

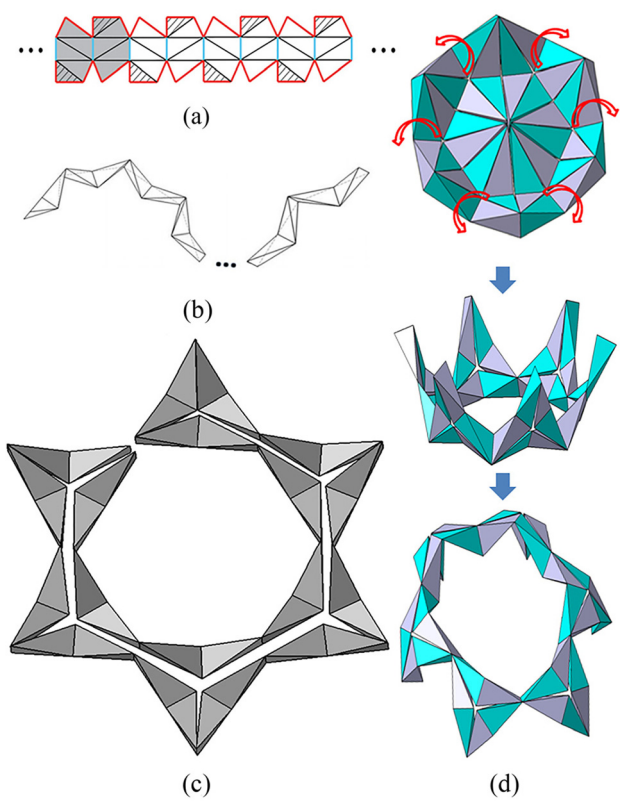

Fig. 14 Fabrication and construction rules for building a hexagram-like mechanism

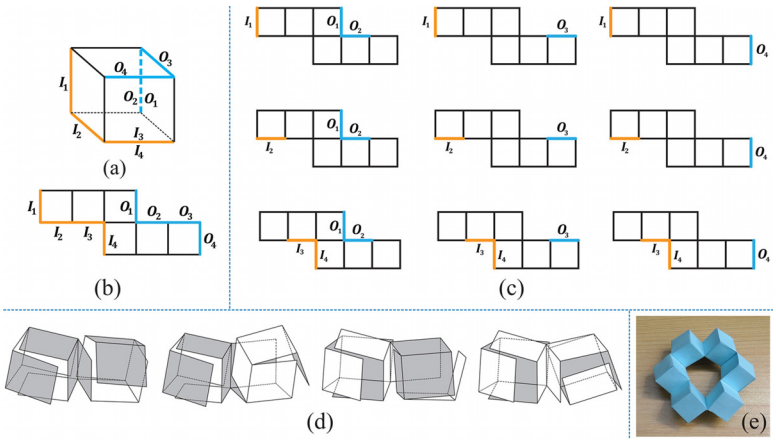

Fig. 15 Fabrication and hinge selection for cubic derivatives

of sheet, then fold each pattern up and obtain a long BSU string shown in Fig. 14(*b*).

(2) Deploy the polyhedral mechanism into a planar configuration: the hexagram-like mechanism into its configuration with six 3stBSUs laying down in Fig. 14(*c*), and the serial cubic ring configuration itself. Then, we select the adjacent hinges based on the skew perpendicularity.
- Tetrahedral BSU has the least hinge selection options in the fact that each tetrahedron is composed of only 2 skew edges. Recall that we geometrically demonstrate 3 representative BSUs with skew perpendicular hinges and their corresponding creases on 2D are synthesized to be linearly arrayed (see the blue lines in Fig. 14(*a*)).
- Unlike tetrahedral BSU patterns, 2 sets of 4 edges on each current cubic BSU pattern (see Fig. 15(*a*)) can be chosen for the hinge coupling the previous BSU pattern, denoted as $I_{1,2,3,4}$, and the hinge, which is coupling the next one, denoted as $O_{1,2,3,4}$. Folding a single cubic BSU pattern gives rise to 3 different spatial hinge-hinge relations defined as follows: (1) *coplanar parallel*: 2 edges functioning as hinges on each cubic unit are within the same surface plane while parallel to each other, such as I_1 and O_1 or I_1 and O_2; (2) *diagonal parallel*: 2 hinges are parallel to each other but sitting along the diagonal direction in a cube, such as I_2 and O_3; (3) *skew perpendicular*: 2 hinges on each cubic unit are neither parallel nor intersecting, but perpendicular to each other, such as I_2 and O_4. Table 1 provides a summary of hinge-hinge spatial geometric relations covering all possible combinations of I_i and O_j, where $i, j = 1, 2, 3, 4$. To ensure a specific deployable kinematic performance, we choose the hinge-hinge combination that results in the skew perpendicularity of adjacent hinge axes. The whole configuration space is enlarged as well by 4 types of different sequential mountain and valley folding at the common hinge of one cubic BSU (Fig. 15(*d*)).

(3) Find an Eulerian cycle starting from one BSU to travel and visit each polyhedral BSU exactly once inside the unfolded configuration. We herein demonstrate again the cycle for the hexagram-like mechanism using aforementioned Algorithm 1 (shown in Figs. 13 and 14(*c*)).

(4) Thread the long folded BSU strings along the path, attach entire disconnected compound joint together, and close all the loops into the final constructs.

Design for Intersection-free Folding Motion: After the Eulerian cycle is generated for a connectivity graph, we cut the cycle at an arbitrary node so that the closed path can always be opened into a straightened string without self-intersection. When considering the volumetric polyhedral linkages instead of edges of negligible thickness, the appropriate synthesis of the predictor of reconfigurability allow us to ensure every continuous folding motion free of intersection. Recall in Sec. 4 that (1) if staying below the rigid state threshold of the vertex angle, the string of tetrahedral BSUs has been proven to be ringed; (2) while enabling the number of BSUs greater than 2, the strings of cubic, prismatic and pyramidal BSU have also been proven to be ringed. That is to say, the intersection between adjacent BSUs occurs if and only if the rigid-state-threshold is designed to be exceeded and units are still chained together in a closed loop. Otherwise, each neighboring BSUs in the Eulerian cycle are sufficient to fit into any local turning or straightening scenario. According to the formation principles, we have discussed for the connectivity graph in Sec. 5.1.1, each constructed polyhedral mechanism is composed of single or multiple loops that topologically allows only ordinary nodes and complex nodes, and geometrically requires adjacent joint axes with skew perpendicularity. Hence, given a specific topological configuration in the connectivity graph, by finding the elementary single-loop with the least edges and constraining the vertex angle from going beyond the rigid-state-threshold, we are guaranteed that the physical BSU string can be folded from a straightened configuration and ringed into loop(s) without intersecting any other BSUs.

5.1.3 Amelioration for Compact Layout Planning. As discussed, each depolyable polyhedral mechanism derived from 4 BSUs reconfigures into a long BSU string and eventually yields a lengthy strip of paper. Hence, we start modifying and re-initiating the 2D layout design on an ideal rectangular-size paper rather

Table 1 Spatial hinge-hinge relation of cubic BSU

Combination	O_1/O_2	O_3	O_4
I_1	coplanar parallel	skew perpendicular	skew perpendicular
I_2	skew perpendicular	diagonal parallel	skew perpendicular
I_3/I_4	skew perpendicular	skew perpendicular	coplanar parallel

than an interminable strip. The fabricating strategies are completed involving another three preparation steps:

(1) As illustrated in Figs. 16(*a*) and 16(*b*), expanding the BSU crease pattern laterally and vertically on a sheet, apply cuts-creases arrangements to each row and zigzag turns between rows. The overall cuts-crease pattern is represented in colors and the operations will proceed in sequence: to cut along *red* lines, fold *black* lines for construct polyhedral links, fold *blue* dashed lines for enclosing additional surfaces, and attach *shaded regions* for adhesion).
(2) Attach 3 sheets together where the top layer remains the original pattern with green-red-purple turning areas, while the rest two layers without the turning areas (see Fig. 16(*c*)).
(3) After cutting, stack down each row gradually by folding the green areas backward and then red areas downward shown in Figs. 16(*a*) and 16(*b*) and eventually lining up a long strip (sequences shown in Fig. 16(*d*)), then folding BSUs into a long string.

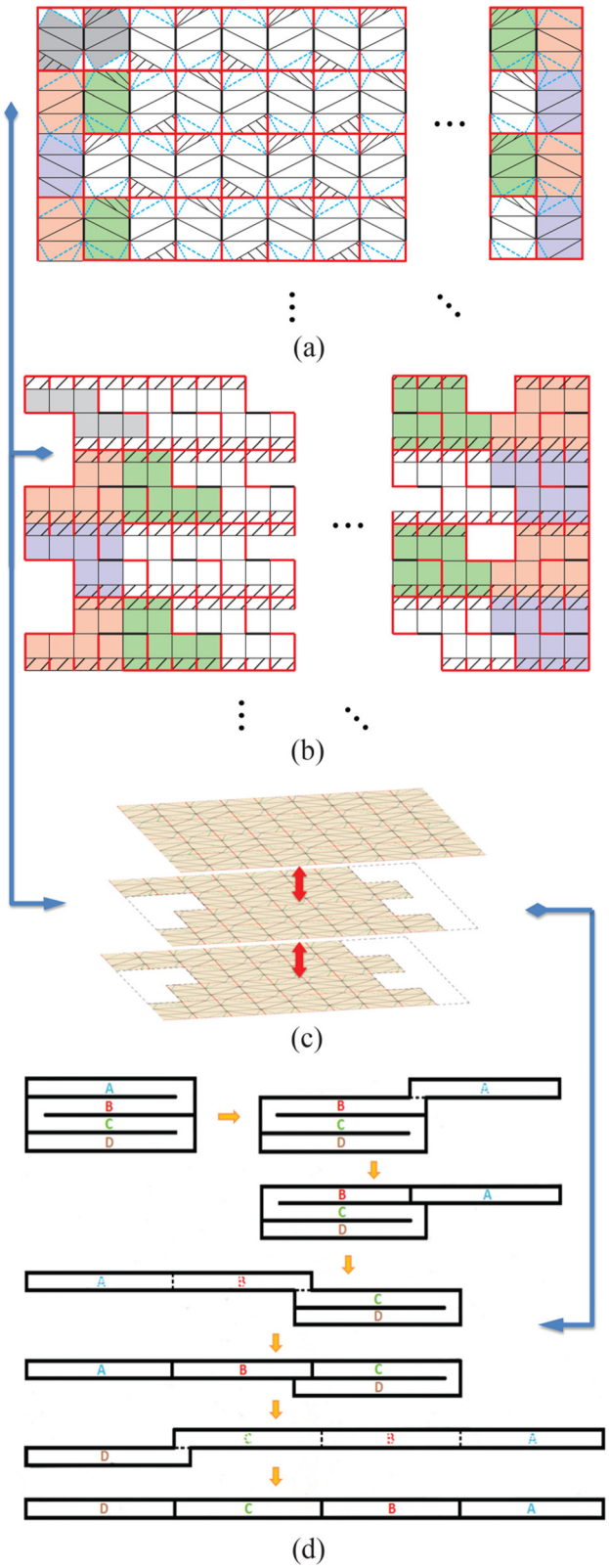

Fig. 16 Ameliorated processes for a compact 2D pattern layout

In step ii, the purpose of the 3-sheets adhesion is to balance the thickness of each polyhedral surface because the turning areas are stacked upon each other three times in the third step as per the row above. We maintain the rectangular paper intact by allowing only line cutting so that: (1) no paper material is wasted (occurs if hollowing out), and (2) the assembly facets are attached inside the tetrahedra and the surface thickness can be increased to enhance structural characteristics such as stiffness and load carrying capacities.

5.2 Multimaterial Printing. The design theories and fabrication concepts of Kinetogami have been proved on the paper substrate. Considering its application in an engineering context, we further explore an alternative substrate which contains anisotropic material properties such as stiffness in planes and high flexural characteristics about hinges. 3D printing technology enables us to achieve this versatile material printed substrate.

Besides paper, a wide variety of nonwovens open up the possibilities for exploring the substrate selection and surface properties (wettability, creasability (wrinkle-resistance), adhesive properties, and stiffness) for a variety of future applications. Flexure joints [26] have been frequently applied in engineering such as self-folding morphing mechanisms [27] and robotic origami [28]. Figure 17(*a*) shows the printed multimaterial sheets where flexural hinges merge with rigid polypropylene facets as produced particularly by Objet Connex 350. The net build size is 320 mm × 108 mm × 1.5 mm and it can be folded fully into a 52 mm × 108 mm × 9 mm package (see Fig. 17(*b*)) without cracking and springing. Deploying the crease pattern and refolding it along with the predesigned snap-fits give one a rotating tetrahedral BSU ring in Figs. 17(*c*) and 17(*d*). Compared to flat contact between the plates and the hinge, the interconnecting cross section shown in Fig. 17(*e*) resolves fatigue cracking and provides more flexibility in the elastomeric joints.

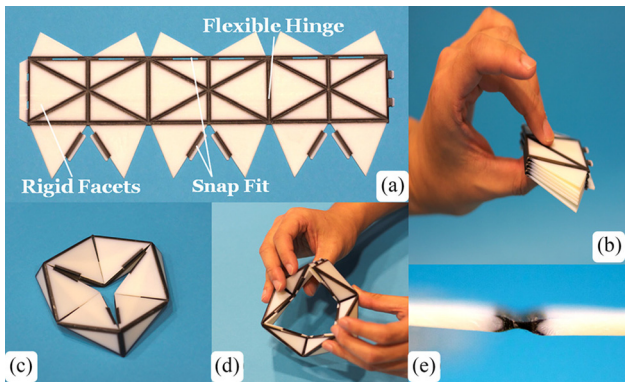

Fig. 17 (*a*) 3D Printed multimaterial sheet, (*b*) compactly flat-folded configuration, (*c*) folded into 6 tetrahedral BSUs in a ring, (*d*) morphed among configurations, and (*e*) flexure hinge

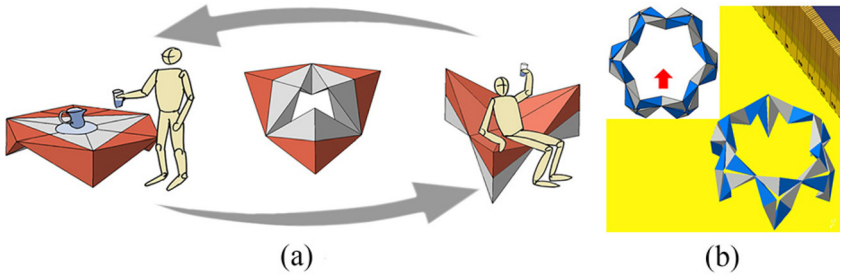

Fig. 18 Visions of (*a*) a multimaterial-printed table reconfigures into a chair (*b*) a hexapod robot with multiple gaits

6 Conclusions and Discussion

In this paper, we have presented a novel folding framework, called "Kinetogami", with multihierarchical and foldable units for the creation of polyhedral mechanisms. We built combinatorial morphing systems by varying the design of individual components in 2D while folding and reconfiguring in 3D. Furthermore, our approach allows designers to synthesize desired reconfigurable motion using measurable design parameters, as the resulting fundamental mathematical basis and spatial perception become accessible. Finally, multimaterial printing technology allows us to integrate rigid facets with interconnecting flexible joints as an alternative material construction that can be folded. The following is our vision of further studies on Kinetogami:

(1) The abilities of Kinetogami enable mechanistic designs by varying layouts, materials on 2D, and hence, providing multiple functionalities in 3D. We find this aspect of applications in the structural and robotic designs to be of great relevance. A vision of a multimaterial printed table mechanism using isos-equal tetrahedral BSUs is shown in Fig. 18(*a*). It can deploy into a chair while reorienting its surface materials to adapt to different load carrying capacities. Another vision of a multigait reconfigurable robot with various locomotive capabilities has been discussed in our previous work [24] (see Fig. 18(*b*)).
(2) One can extend computer support to ease the realization of this new science-based art form. We have demonstrated the foldable and reconfigurable mechanisms using a hands-on construction. Computational algorithms and tools can further help one unfamiliar with the geometric nuances to design, analyze, and optimize Kinetogamic structural and mobile forms, as well as the folding process plan.
(3) Through explorations at the intersections of art-science-geometry and digital information technologies, we intend to promote imagination and critical thinking.

Acknowledgment

The authors of this paper would like to acknowledge the support by Donald W. Feddersen Chair professorship that enabled Wei to participate in developing this area. We would also like to thank Professor Rebecca Kramer for her comments.

Nomenclature

θ = measurable vertex-angle variable in isosceles tetra-facets
n = number of isosceles tetra-BSUs in a single closed loop
α, β, γ = the vertex angle in each side of the tetrahedron

References

[1] Arkin, E. M., Bender, M. A., Demaine, E. D., Demaine, M. L., Mitchell, J. S., Sethia, S., and Skiena, S. S., 2004, "When Can You Fold a Map?," Comput. Geom., **29**(1), pp. 23–46.
[2] Demaine, E., Demaine, M., and Mitchell, J. S., 2000, "Folding Flat Silhouettes and Wrapping Polyhedral packages: New Results in Computational Origami," Comput. Geom., **16**, pp. 3–21.
[3] Lang, R. J., 1998, TreeMaker 4.0: A Program for Origami Design.
[4] Demaine, E., and Tachi, T., 2010, "Origamizer: A Practical Algorithm for Folding Any Polyhedron," Manuscript.
[5] Miura, K., 2009, "The Science of Miura-Ori: A Review," 4th International Meeting of Origami Science, Mathematics, and Education, R. J. Lang, ed., A K Peters, Natick, MA, pp. 87–100.
[6] Hoffman, R., 2001, "Airbag Folding: Origami Design Application to an Engineering Problem," 3rd International Meeting of Origami Science, Mathematics, and Education.
[7] You, Z., and Kuribayashi, K., 2003, "A Novel Origami Stent," Proceedings of Summer Bioengineering Conference.
[8] Fischer, S., Drechsler, K., Kilchert, S., and Johnson, A., 2009, "Mechanical Tests for Foldcore Base Material Properties," Composites, Part A, **40**, pp. 1941–1952.
[9] Mullineux, G., Feldman, J., and Matthews, J., 2010, "Using Constraints at the Conceptual Stage of the Design of Carton Erection," Mech. Mach. Theory, **45**(12), pp. 1897–1908.
[10] Gurkewitz, R., and Arnstein, B., 2003, *Multimodular Origami Polyhedra: Archimedeans, Buckyballs, and Duality*, Dover, New York.
[11] Hart, G., 2007, "Modular Kirigami," Proceedings of Bridges Donostia.
[12] Griffith, S., 2004, "Growing Machines," Ph.D. thesis, MIT, MA.
[13] Cheung, K., Demaine, E., Bachrach, J., and Griffith, S., 2011, "Programmable Assembly With Universally Foldable Strings (Moteins)," IEEE Trans. Rob. Autom., **27**(4), pp. 718–729.
[14] Demaine, E., Demaine, M., Lindy, J., and Souvaine, D., 2005, "Hinged Dissection of Polypolyhedra," Lect. Notes Comput. Sci., **3608**, pp. 205–217.
[15] Demaine, E., Demaine, M., Eppstein, D., Frederickson, G., and Friedman, E., 2005, "Hinged Dissection of Polyominoes and Polyforms," Comput. Geom.: Theory Appl., **31**(3), pp. 237–262.
[16] Goldberg, M., 1942, "Polyhedral Linkages," Math. Mag., **16**(7), pp. 323–332.
[17] Gilpin, K., Kotay, K., Rus, D., and Vasilescu, L., 2008, "Miche: Modular Shape Formation by Self-Disassembly," Int. J. Robot. Res., **27**(3), pp. 345–372.
[18] Ke, Y., Ong, L., Shih, W., and Yin, P., 2012, "Three-Dimensional Structures Self-Assembled From DNA Bricks," Science, **338**(6111), pp. 1177–1183.
[19] Schatz, P., 1998, *Rhythmusforschung und Technik*, Verlag Freies Geistesleben, Stuttgart.
[20] Sehattsehneide, D., and Walker, W., 1977, *M.C.Eseher Kalerdoeycels*, BallantineBooks, NewYork.
[21] Chen, Y., You, Z., and Tarnai, T., 2005, "Threefold-Symmetric Bricard Linkages for Deployable Structures," Int. J. Solids Struct., **42**(8), pp. 2287–2301.
[22] Baker, E., 1980, "An Analysis of Bricard Linkages," Mech. Mach. Theory, **15**, pp. 267–286.
[23] Chen, Y., and You, Z., 2012, "Spatial Overconstrained Linkages—The Lost Jade," Hist. Mech. Mach. Sci., **15**, pp. 535–550.
[24] Gao, W., Ramani, K., and Cipra, R. J., 2012, "Reconfigurable Foldable Spatial Mechanisms and Robotic Forms Inspired by Kinetogami," Proceedings of the ASME 2012 IDETC/CIE.
[25] Milgram, R., 1974, "Surgery With Coefficients," Ann. Math., **100**(2), pp. 194–248.
[26] Kang, B., Wen, J., Dagalakis, N., and Gorman, J., 2004, "Analysis and Design of Parallel Mechanisms With Flexure Joints," Proceedings of IEEE International Conference on Robotics and Automation.
[27] Zotov, S., Rivers, M., Trusov, A., and Shkel, A., 2010, "Chip-Scale IMU Using Folded-MEMS Approach," IEEE Sens. J., pp. 1043–1046.
[28] Hawkes, E., An, B., Benbernou, N. M., Tanaka, H., Kim, S., Demaine, E. D., Rus, D., and Wood, R. J., 2010, "Programmable Matter by Folding," Proc. Natl. Acad. Sci. U.S.A., **107**(28), pp. 12441–12445.